



OPEN ACCESS

EDITED BY

Housseem Jerbi,
University of Hail, Saudi Arabia

REVIEWED BY

Lei Zhang,
Beijing Institute of Technology, China
Mourad Kchaou,
University of Hail, Saudi Arabia
Rabeh Abbassi,
University of Hail, Saudi Arabia

*CORRESPONDENCE

Jingjing Feng,
✉ hyui451214@163.com

RECEIVED 26 February 2024

ACCEPTED 27 June 2024

PUBLISHED 24 July 2024

CITATION

Feng J (2024), Parameter fuzzy rectification for sliding mode control of five-phase permanent magnet synchronous motor speed control system.

Front. Mech. Eng 10:1391593.
doi: 10.3389/fmech.2024.1391593

COPYRIGHT

© 2024 Feng. This is an open-access article distributed under the terms of the [Creative Commons Attribution License \(CC BY\)](https://creativecommons.org/licenses/by/4.0/). The use, distribution or reproduction in other forums is permitted, provided the original author(s) and the copyright owner(s) are credited and that the original publication in this journal is cited, in accordance with accepted academic practice. No use, distribution or reproduction is permitted which does not comply with these terms.

Parameter fuzzy rectification for sliding mode control of five-phase permanent magnet synchronous motor speed control system

Jingjing Feng*

Department of Electrical and Electronic Engineering, Suzhou College of Information Technology, Suzhou, China

Introduction: Nowadays, five-phase permanent magnet synchronous motors have been widely used in the industrial and transportation fields, and the existing sliding mode control methods for speed control systems can no longer meet the requirements such as fast response and good stability.

Methods: In light of the aforementioned considerations, the study initially employs mathematical modeling to elucidate the five-phase permanent magnet synchronous motor. Secondly, on the basis of proportional-integral-derivative sliding mode control, radial basis function and Takagi-Sugeno-Kang fuzzy model are introduced for parameter identification and optimization and regulation. Finally, a new neural network regulation algorithm and speed control strategy are proposed.

Results and Discussion: The experimental results demonstrated that the expected parameter optimization rate of the regulation algorithm can reach 90%, and the overshooting amount under small inertia working condition is only 3%, and the adjustment time is 0.02 s. The new control algorithm can be used to control the motor speed with the lowest speed fluctuation and the fastest recovery time. In addition, when affected by the load torque, the motor speed controlled by the new strategy fluctuated the least, with a speed drop of only 1% and the fastest recovery time of 0.02 s. It exhibited the lowest control error of 3.7% and the lowest overshooting amount of 5.9%.

Conclusion: In summary, the suggested approach has the potential to significantly enhance the speed control system's control performance while maintaining strong resilience and anti-interference capabilities. The method has certain guiding significance for the practical application of five-phase permanent magnet synchronous motor speed control system.

KEYWORDS

five-phase permanent magnet synchronous motor, speed control system, sliding mode control, parameter tuning, fuzzy models

1 Introduction

Five-phase Permanent Magnet Synchronous Motor (FPMSM) has become an indispensable power source in industrial automation and modern transportation systems due to its high efficiency and excellent performance (Xu et al., 2020). With the advancement of technology and the growth of industrial demands, the need for precise control of motor speed control systems is increasing, and the selection of appropriate control strategies becomes particularly critical. Although conventional control methods, such as smooth-mode control, have been widely used in these systems, they often exhibit performance degradation in response to variations in system parameters and external perturbations, which poses a significant challenge in maintaining system responsiveness and stability (Hou et al., 2020; Xu et al., 2021). To solve this problem, numerous researchers have tried various control strategies, including empirical, trial-control and optimization methods, to improve the parameter settings of the sliding mode controller. Among the aforementioned methods, the empirical and trial-control methods rely on experimentation and debugging to obtain the initial values of the controller parameters. However, these methods are not only complicated to operate, but also have limited effects. Currently, the optimization method mainly solves for the optimal controller parameters under specific performance indexes through algorithms. Nevertheless, its parameter tuning remains challenging in the face of nonlinear and changing system environments (Liu et al., 2020). Therefore, the study innovatively proposes an improved Proportional-Integral-Derivative (PID) sliding mode control method by introducing machine learning optimization techniques, especially Radial basis function algorithm (RBF) and Takagi-Sugeno-Kang (TSK) fuzzy model. Derivative, PID sliding mode control method. The method aims to significantly improve the performance and adaptability of FPMSM speed control system. This research is divided into four parts, the first part is the analysis and summary of others' research, the second part describes how the FPMSM mathematical model and parametric fuzzy regularization strategy are constructed, respectively, while the third part tests the performance of this new method, and the last part concludes the article.

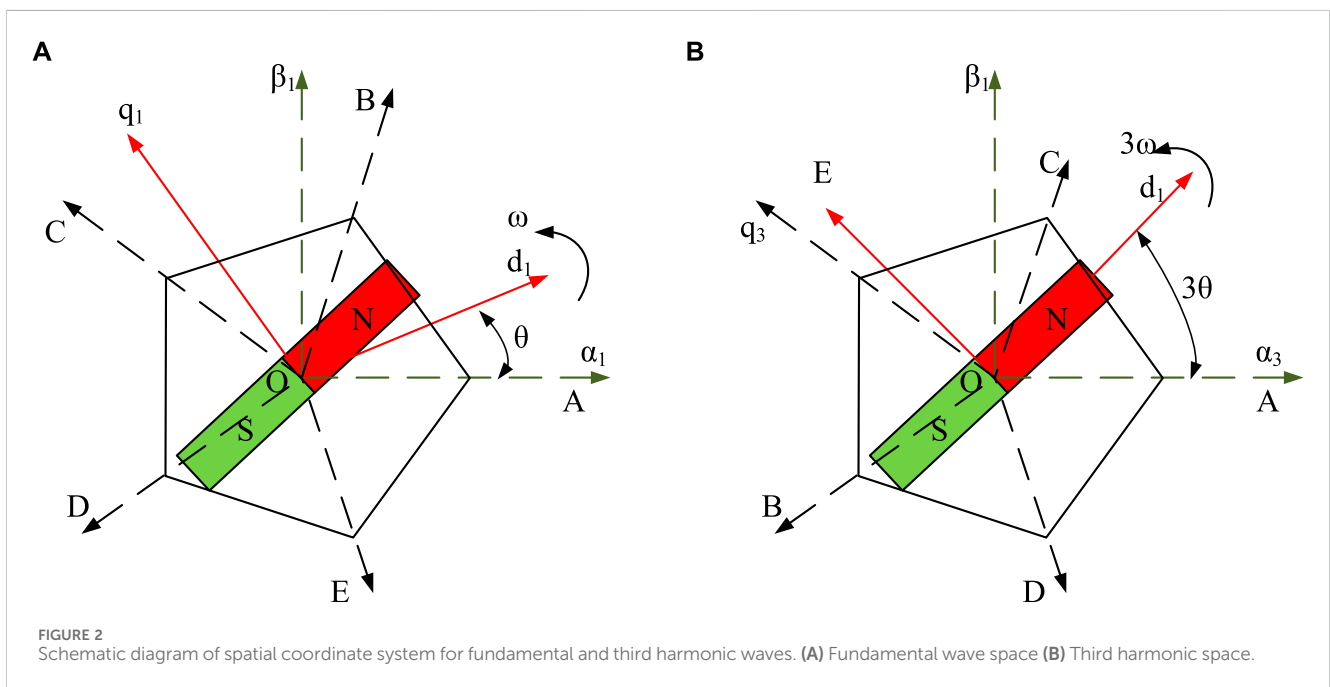
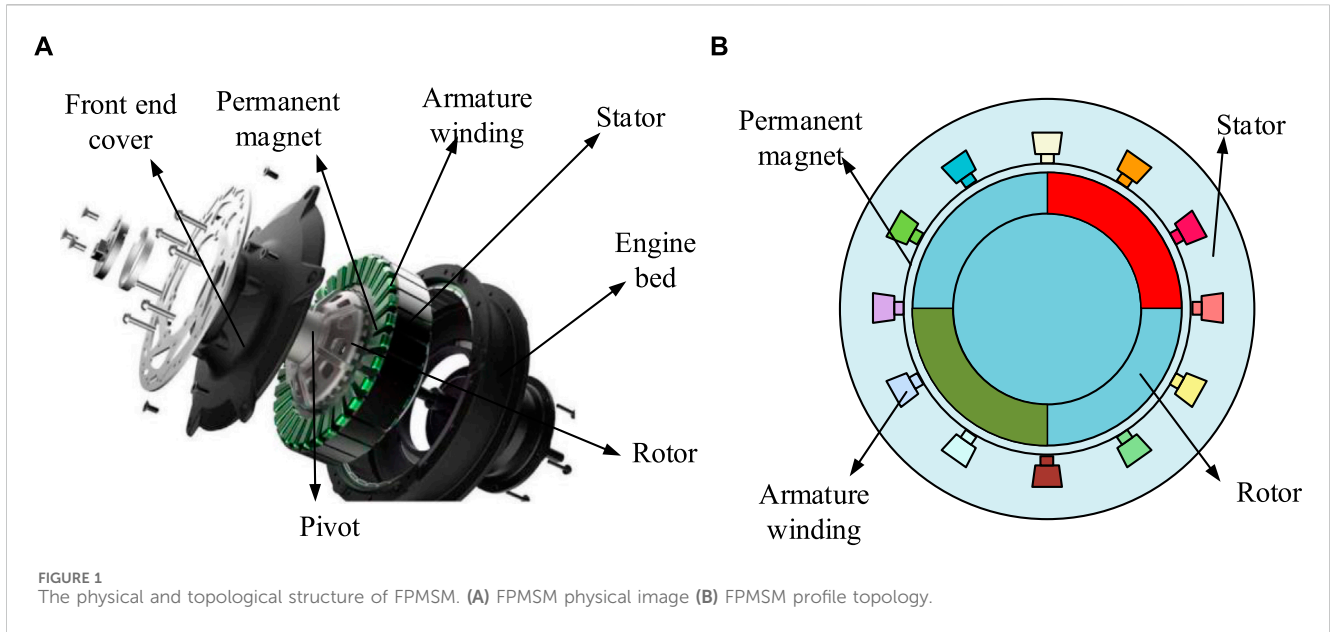
2 Related works

With the benefits of high torque precision, high power density, and high efficiency, FPMSM is a novel kind of high-performance motor. Due to its nonlinear and coupling characteristics, the study of SMC strategy for its SCS is of great significance. In order to explore a novel SMC strategy for FPMSM speed regulation, Sun et al. (2022) proposed a speed decoupling control strategy after combining dual-frequency vector modulation. The experimental results showed that the effectiveness of the strategy in the simulation test trial set was high and the control accuracy was good (Sun et al., 2022). Li et al. (2022) found that in field-oriented controlled FPMSM drives, the current sensors may fail in harsh operating environments, which can lead to data diagnostic crashes in the motor SCS. Therefore, the research team proposed a novel SCS current sensor fault-tolerant control strategy after combining the theory of third harmonic control. Experimental results showed that the strategy has good

control robustness over the entire speed range (Li et al., 2022). To explore a new FPMSM SMC PT strategy, Mossa et al. (2022) proposed a novel vector controller for the drive after combining sliding mode and adaptive system. The experimental results demonstrated that this controller has better enhancement performance and is able to reduce the deviation between resistance and stator inductance compared to a single adaptive system (Mossa et al., 2022). Junejo et al. (2020) suggested a new adaptive terminal sliding mode convergence law to enhance the speed control performance of FPMSM under internal and external disturbances. The experimental results indicated that this new convergence law significantly outperforms the conventional convergence law on the Lyapunov function and is more feasible (Junejo et al., 2020).

Parameter fuzzy tuning refers to the adjustment of the control parameters of a system so that it can maintain stable operation or meet predetermined performance requirements under uncertain environmental conditions. Due to the complexity and variability of FPMSM's PT, the appropriate parameters need to be determined based on the characteristics and control requirements of the specific system. Hussain discovered that in vector controlled permanent magnet synchronous motor drives, it is challenging to set the current control parameters. Consequently, the researcher suggested a generalized PT design approach. The method's applicability and robustness in terms of tracking, disturbance suppression, and noise sensitivity were demonstrated by the experimental results (Hussain, 2020). Bi et al. (2022) concluded that optimizing control parameters is important for the high-performance operation of FPMSM drives. Therefore, they proposed a parameter self-correction method after combining multi-objective optimization and online tracking. The experimental results demonstrated that this method is more capable of realizing the online tracking of control and observation parameters compared to the traditional PT method (Bi et al., 2022). Li et al. (2021) found that the dependence of differential beat-free predictive current control on the accuracy of FPMSM parameters is the main obstacle to its wide application. They therefore suggested a novel control strategy in order to address the issue. According to the experimental data, this strategy was significantly more effective than other conventional methods under complex parameter mismatch settings (Li et al., 2021). Xia J. et al. (2020) concluded that there are abnormal perturbations in the electrical and mechanical parameters of the FPMSM under different operating conditions, which can greatly degrade the control performance. Therefore, they proposed a robust control strategy with parameter adaptation. Experimental results demonstrated that this strategy can realize robust regulation of stator current and rotor speed while accurately estimating the machine parameters (Xia J. et al., 2020).

In conclusion, researchers both domestically and internationally have investigated the SCS SMC of motors and the PT within FPMSM to varying degrees in recent years, and they have suggested several useful control schemes and PT techniques. However, with the development of technology, the traditional PT method of SMC can no longer meet the demand, therefore, the research tries to innovate the fuzzy rectification of the parameters of the SCS SMC of FPMSM, and innovatively improves the RBF and the TSK jointly, which is used to optimize the parameter control of the PID SMC.



3 Fuzzy improved neural network-based parameter tuning for smooth mode control of motor speed control

To construct a reasonable PT method for SMC of motor speed control, the study firstly performs mathematical modeling for FPMSM under hypothetical state. Secondly, the traditional PID SMC is optimized, and the RBF algorithm is introduced for parameter identification. Finally, a TSK fuzzy neural network is incorporated for PT calculation and a novel FPMSM motor speed SMC strategy is proposed.

3.1 Mathematical modeling of FPMSM for vector control

FPMSM is a synchronous motor that uses permanent magnet material as an excitation source. It generates a rotating magnetic field through five sets of coils on the stator, which interacts with the magnetic field of the permanent magnets on the rotor to achieve the rotation of the rotor (Long et al., 2020; Yang et al., 2021). Its SCS is characterized by high order, nonlinearity and strong coupling. The physical and topological structure of FPMSM is shown in Figure 1.

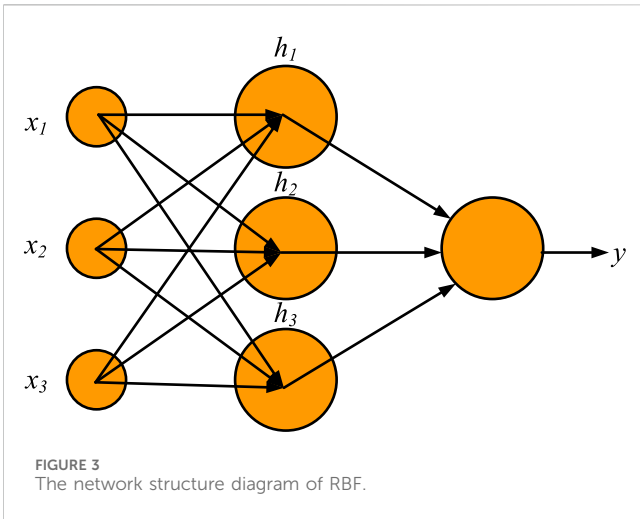


Figure 1A shows the physical view of the FPMSM and Figure 1B shows the sectional topology of the FPMSM. In Figure 1, the rotor surface is covered with tile-like permanent magnets, while the rotor itself is not configured with windings (Choudhuri et al., 2023). In the stator slot, the layout of the five-phase centralized windings expresses the independence of the magnetic circuits between the phases through mathematical modeling. Specifically, the coupling coefficients between the inductances of each phase are minimized by a sophisticated physical design, which effectively reduces mutual inductance and thus improves the accuracy of the model (Zhao et al., 2021). In addition, the slotting effect is usually ignored in the general model simplification because it

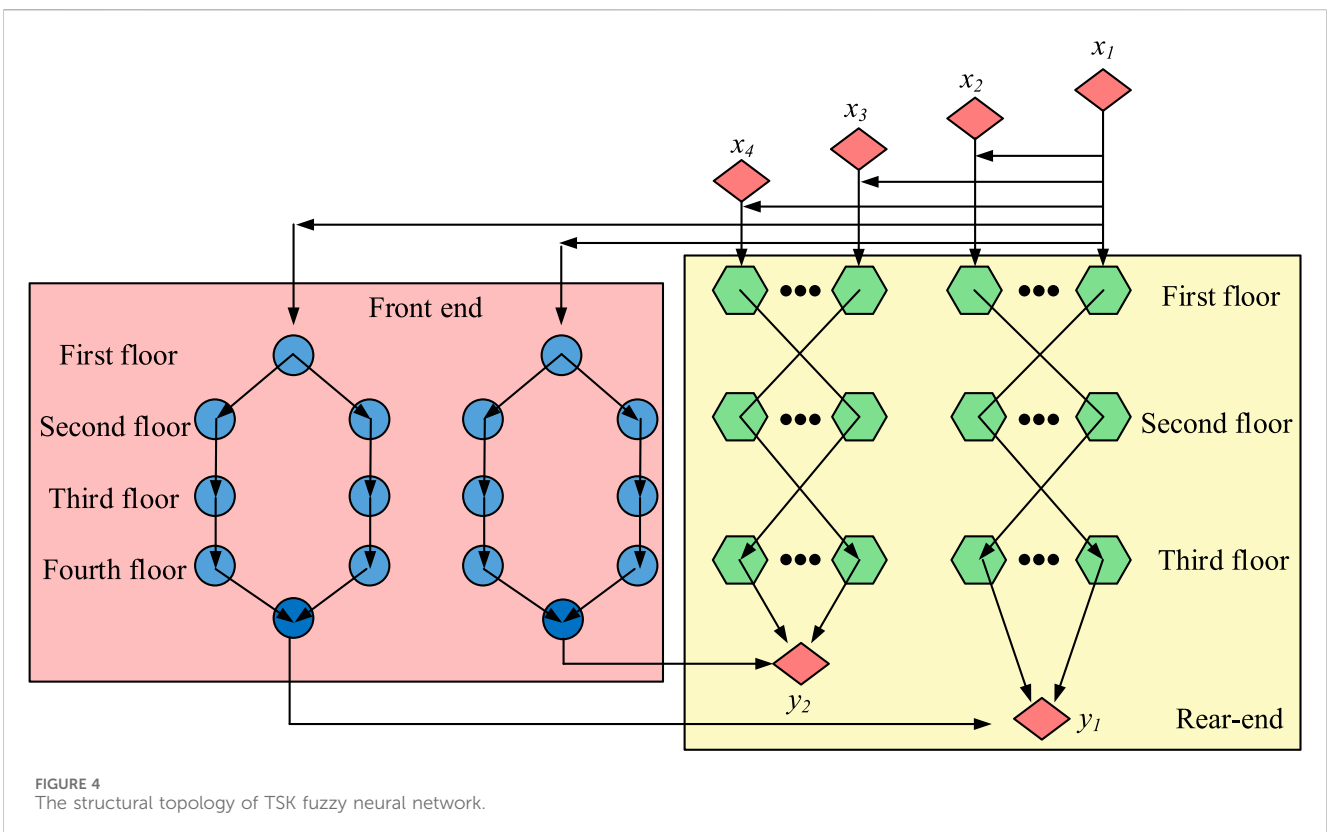
introduces additional harmonics which increase electromagnetic noise and vibration and reduce the smoothness of the motor operation. On the contrary, magnetic circuit saturation is taken into account, which has a significant effect on the electromagnetic characteristics of the motor. A nonlinear magnetic circuit model is used in motor design to approximate the magnetic circuit saturation, taking into account its effect on efficiency and output torque. This nonlinear analysis helps to improve the prediction accuracy of the model under high load conditions. Therefore, the study, in order to simplify the analysis, adopts a hypothetical treatment, i.e., it assumes that the motor of the FPMSM is star connected and symmetrical, while ignoring the effects brought about by the conductivity of the permanent magnets, core saturation, and hysteresis and eddy currents. At this stage, the FPMSM is equivalently represented in terms of Pike's matrix and Clark's matrix for the stationary coordinate system (CS) and the natural CS, respectively. Where the voltage equation in the natural CS is shown in Eq. 1.

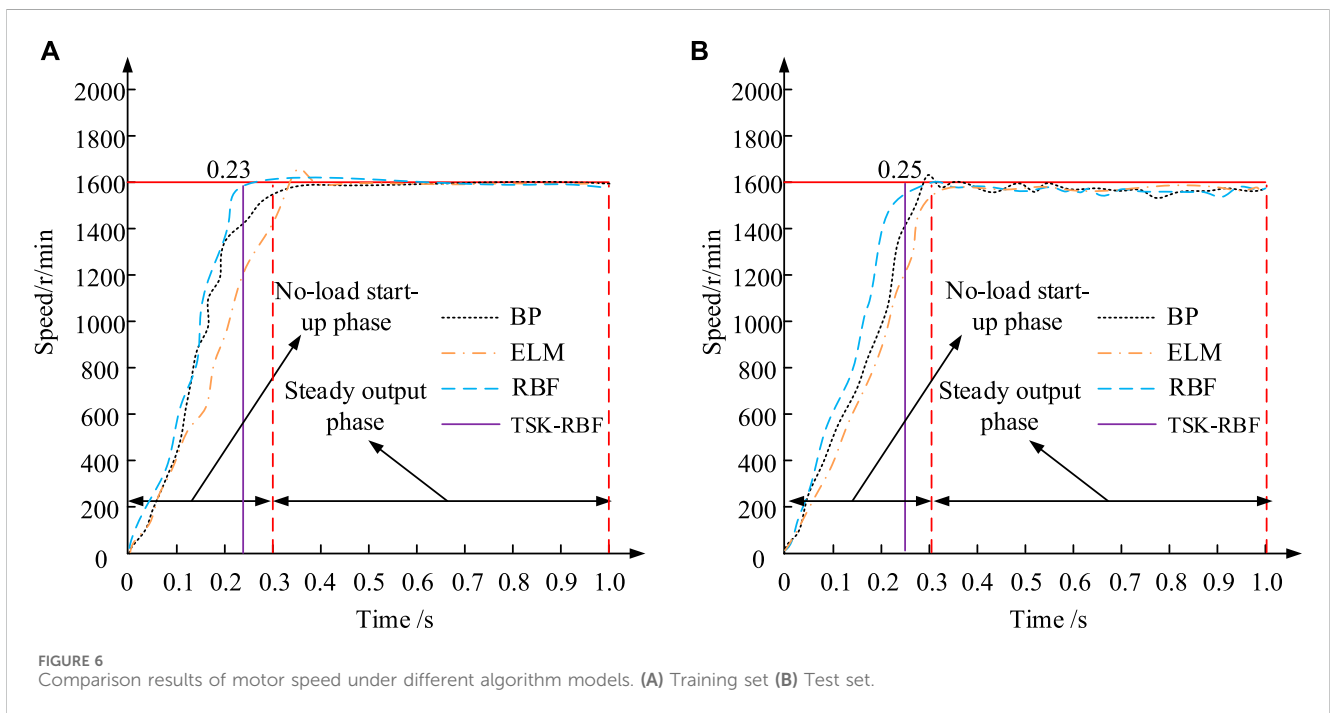
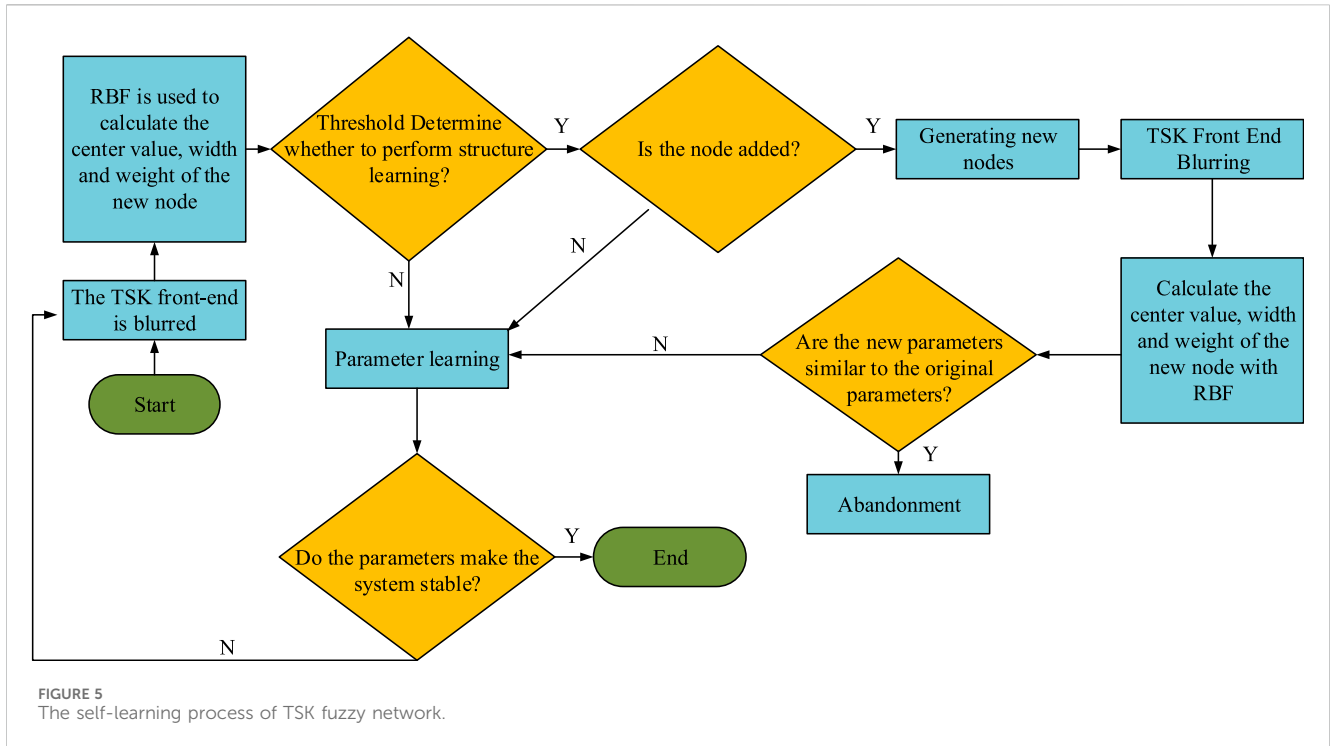
$$U_{si} = R_s i_{si} + \frac{d\lambda_{si}}{dt} \tag{1}$$

In Eq. 1, U_{si} denotes the voltage of item i , R_s denotes the stator resistance. i_{si} denotes the current of item i , and λ_{si} denotes the magnetic chain of item i . d denotes the differential operation symbol and t denotes the time. The equation of the magnetic chain is calculated as shown in Eq. 2.

$$\lambda_{si} = L_s i_{si} + \lambda_{pmi} \tag{2}$$

In Eq. 2, L_s denotes the stator self-inductance and λ_{pmi} denotes the magnetic chain generated by the permanent magnets. The electromagnetic torque (EMT) equation is shown in Eq. 3.





$$T_e = \frac{P}{2} \sum_{i=1}^5 (i_{si} \times \lambda_{pmi}) \quad (3)$$

In Eq. 3, T_e denotes the EMT and P denotes the pole logarithm. The equation of mechanical motion is shown in Eq. 4.

$$J \frac{d\omega}{dt} = T_e - T_l - B\omega \quad (4)$$

In Eq. 4, J denotes the rotational inertia and ω denotes the rotational speed. T_l is the load torque and B denotes the friction

coefficient. It is evident from the preceding equations that there is mutual interaction between the intersecting and straight axes in the mathematical model of the FPMSM's natural CS. This coupling nature makes it challenging to precisely control the speed and EMT of the motor. The process involves the dynamic response of the motor, including starting, braking and sudden load changes. And the dynamic equations take into account the rotational inertia and friction of the rotor and how quickly it responds to control commands and load changes. Therefore, decoupling the five-

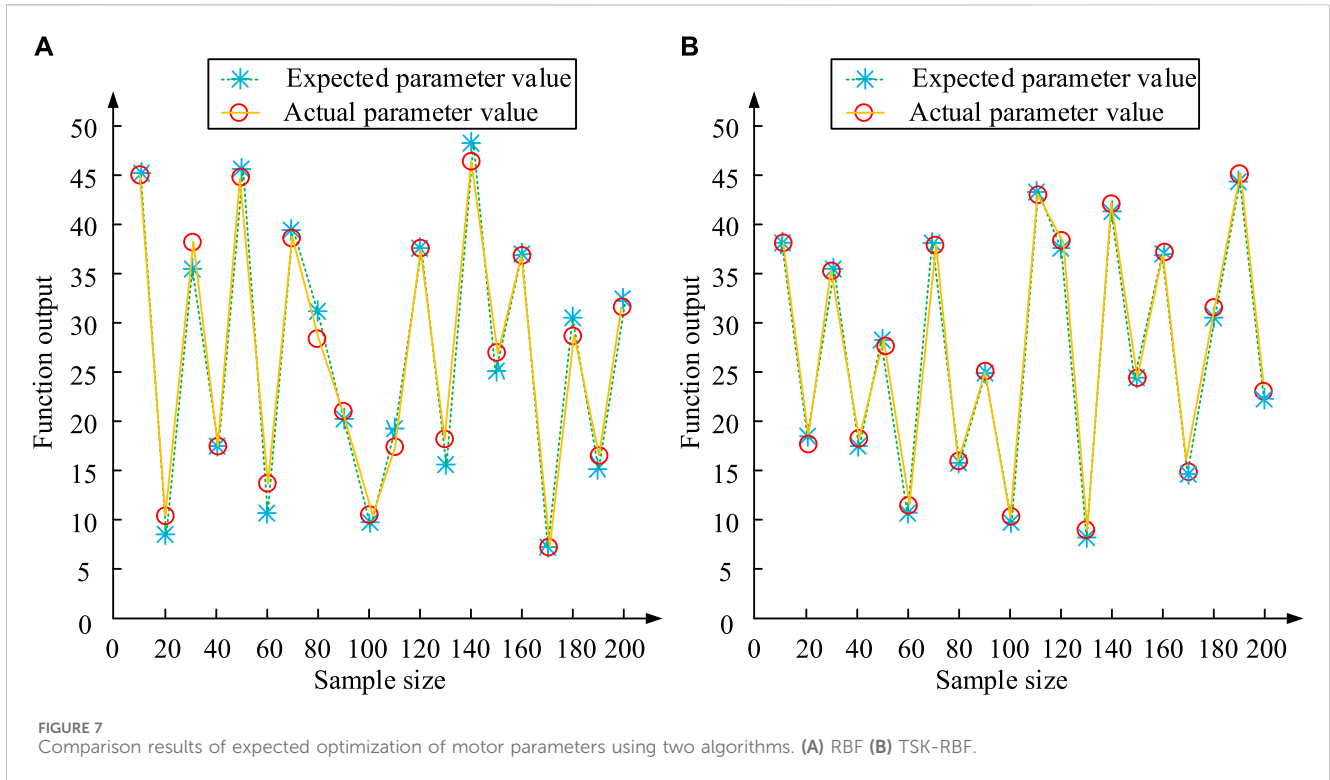


TABLE 1 Test results of indicators for different algorithm controllers.

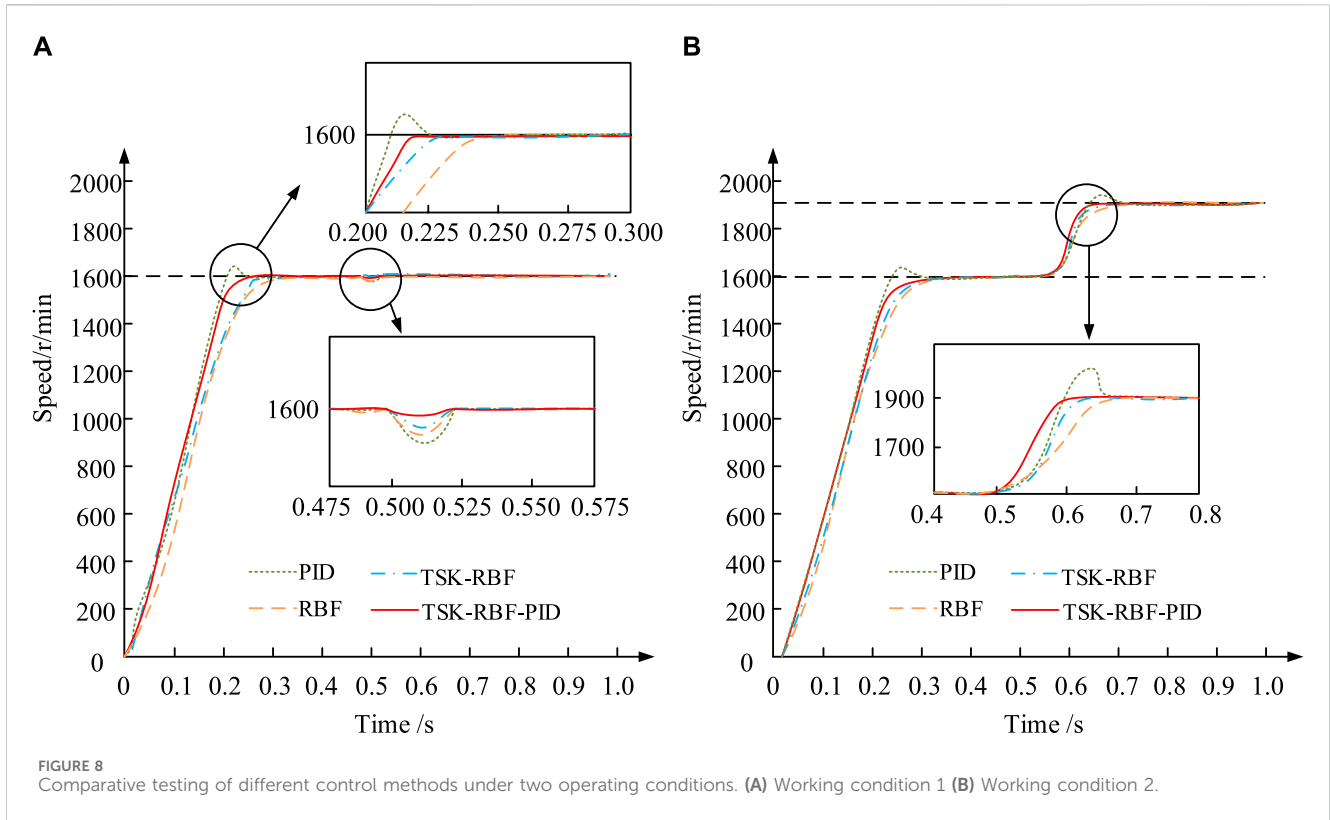
| Working condition | Controller | Overshoot/% | Adjustment time/s |
|-------------------|---------------|-------------|-------------------|
| Small inertia | BP | 30 | 0.14 |
| | ELM | 22 | 0.09 |
| | RBF | 12 | 0.05 |
| | Literature 18 | 5 | 0.04 |
| | TSK-RBF | 3 | 0.02 |
| Large inertia | BP | 65 | 0.27 |
| | ELM | 47 | 0.16 |
| | RBF | 29 | 0.09 |
| | Literature 18 | 12 | 0.07 |
| | TSK-RBF | 8 | 0.04 |

phase PMSM model for order reduction is necessary to simplify the analysis process. The study is carried out to transform in the manner of Clark's and Pike's matrices to obtain the physical mapping relations in the two-phase CS with constant amplitude. Where Figure 2 displays the spatial CS of the fundamental and third harmonic.

In Figure 2, $A - B - C - D - E$ is a five-term stationary CS with two neighboring systems separated by 72° . $\alpha_1 - \beta_1$ and $d_1 - q_1$ denote the stationary and rotational CSs in the fundamental wave space, and $\alpha_3 - \beta_3$ and $d_3 - q_3$ denote the stationary and rotational CSs in the third harmonic space, respectively. This study applies the principle of invariance of the magnetic momentum to obtain the Clark's and

Pike's matrices for the transformation of the five natural CSs to the stationary CS, based on the relationship of each physical quantity in the fundamental wave space and the third harmonic space. The matrix equations are displayed in Eq. 5.

$$T = k \begin{cases} 1 & \cos \alpha & \cos 2\alpha & \cos 3\alpha & \cos 4\alpha \\ 0 & \sin \alpha & \sin 2\alpha & \sin 3\alpha & \sin 4\alpha \\ 1 & \cos 3\alpha & \cos 6\alpha & \cos 9\alpha & \cos 12\alpha \\ 0 & \sin 3\alpha & \sin 6\alpha & \sin 9\alpha & \sin 12\alpha \\ \frac{1}{2} & \frac{1}{2} & \frac{1}{2} & \frac{1}{2} & \frac{1}{2} \end{cases} \quad (5)$$



In Eq. 5, k denotes the constraint coefficient. Considering that this study takes the positively rotating wound motor as a reference, the effect of the third harmonic component on the motor performance can be neglected. At this time, the Pike transform matrix is shown in Eq. 6.

$$C_{ris} = \begin{cases} \cos \theta & \sin \theta & 0 & 0 & 0 \\ -\sin \theta & \cos \theta & 0 & 0 & 0 \\ 0 & 0 & 1 & 0 & 0 \\ 0 & 0 & 0 & 1 & 0 \\ 0 & 0 & 0 & 0 & 1 \end{cases} \quad (6)$$

Eqs 5, 6 describe the vector control strategy for the five-phase motor in detail, including its mathematical derivation and implementation details. The control algorithm then utilizes the Pike and Clark matrices for coordinate transformation to accurately control the amplitude and phase of the current to achieve precise regulation of the electromagnetic torque. The equations for the stationary CS voltage and EMT at this point after transformation are shown in Eq. 7.

$$\begin{cases} u_\alpha = R_s i_\alpha + \frac{d\lambda_\alpha}{dt} \\ u_\beta = R_s i_\beta + \frac{d\lambda_\beta}{dt} \end{cases}; T'_e = \frac{3}{2} P (\lambda_\alpha i_\beta - \lambda_\beta i_\alpha) \quad (7)$$

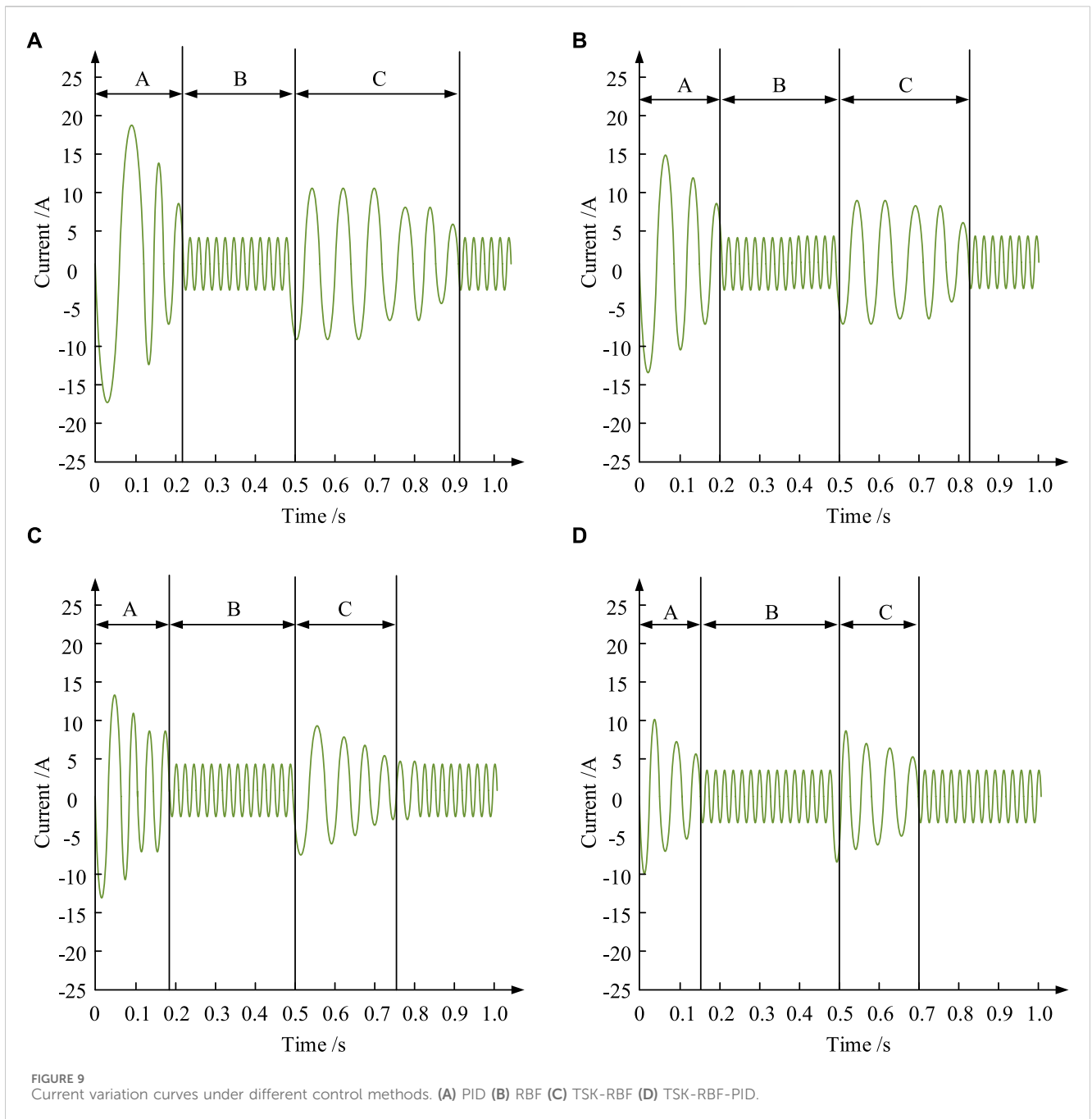
The stationary CS voltages at this point after transformation and in Eq. 7, u_α and u_β denote the voltages on the α and β axes, respectively, in the stationary CS. i_α and i_β denote the currents on the α and β axes, respectively, in the stationary CS. λ_α and λ_β denote the magnetic chains on the α and β axes, respectively. The EMT equation is shown in Eq. 7.

3.2 Parameter tuning for fuzzy improved RBF-based sliding mode PID control

Sliding mode PID control is an advanced control strategy that combines the robustness of SMC with the simplicity of PID control, and this control method is particularly effective in dealing with uncertainty and nonlinear systems (Xia X. et al., 2020; He et al., 2020). Nevertheless, at specific instances, the fixed and unchanging control parameters are unable to fulfill the demands of working conditions with high requirements. Consequently, the study selects the more classical RBF algorithm for nonlinear data fitting approximation, with the objective of compensating for the shortcomings of Sliding Mode PID control. In Figure 3, the RBF network structure is displayed (Zheng et al., 2022).

The approach in Figure 3 transfers the input space to a high-dimensional feature space, which allows for the linear divisibility of a linearly indivisible issue (He et al., 2022). In PID for SMC, the RBF infinitely approximates the optimal sliding mode PID control scheme by continuously correcting its own output weights, centroid positions and expansion constants. Where the correction equation of RBF in gradient descent method for each node parameter is shown in Eq. 8.

$$\begin{cases} \nabla w_j = -\eta \frac{\partial E}{\partial w_j} \\ \nabla c_{ij} = -\eta \frac{\partial E}{\partial c_{ij}} \\ \nabla \sigma_j = -\eta \frac{\partial E}{\partial \sigma_j} \end{cases} \quad (8)$$



In Eq. 8, E denotes the error function, usually the root mean square error. η denotes the learning rate, $c_{i'j}$ denotes the i' th dimension centroid of the j th RBF neuron. σ_j denotes the width constant of the j th neuron, and w_j denotes the weight of the j th output neuron. A single RBF neural network is not fast enough for parameter selection by cross-validation alone. The study further introduces the TSK model, which differs from the traditional fuzzy neural model in that it employs a linear function in the conclusion part of each rule, rather than a fuzzy set. This design is more efficient and accurate in realizing fuzzy control and approximating nonlinear functions. Figure 4 displays the TSK fuzzy neural network's structural architecture (Abbassi et al., 2022).

In Figure 4, the whole TSK fuzzy neural network can be divided into a front-end with fuzzy rule storage and a back-end composed of constructing fuzzy rules. It has an input layer, a fuzzification layer, a rule layer, a defuzzification layer, and an output layer. It also incorporates neural network and TSK fuzzy model features (Abbassi et al., 2023). Data is fed into the input layer, which then fuzzifies it into fuzzy values, applies fuzzy logic rules, defuzzifies the rule output, packages it, and outputs findings that are easy to understand. This structure makes the network suitable for dealing with complex nonlinear problems with good interpretability. Where the fuzzification layer is calculated as shown in Eq. 9.

TABLE 2 Indicator test results of rolling bearings under different control methods.

| Condition | Bearing test serial number | PID (Control error/ %/Overshoot/%) | RBF (Control error/ %/Overshoot/%) | TSK-RBF (Control error/ %/Overshoot/%) | TSK-RBF-PID (Control error/ %/Overshoot/%) |
|---------------------|----------------------------|------------------------------------|------------------------------------|--|--|
| Working condition 1 | 1 | 27.4/51.3 | 22.8/39.8 | 11.7/17.6 | 3.9/5.9 |
| | 2 | 25.1/45.8 | 20.7/37.4 | 18.5/22.4 | 4.2/6.8 |
| | 3 | 22.3/43.1 | 18.9/34.5 | 15.7/27.5 | 3.7/9.8 |
| | 4 | 19.2/37.8 | 16.8/22.4 | 16.2/17.6 | 4.1/6.3 |
| | 5 | 19.8/38.9 | 18.1/29.4 | 13.4/29.8 | 3.9/6.1 |
| Working condition 2 | 1 | 27.6/47.3 | 25.4/38.6 | 16.7/23.7 | 5.1/9.7 |
| | 2 | 19.8/48.7 | 17.5/37.6 | 17.4/23.5 | 5.3/8.4 |
| | 3 | 18.4/41.2 | 16.7/29.6 | 15.3/19.7 | 6.2/6.7 |
| | 4 | 19.4/34.3 | 18.5/24.5 | 13.2/19.4 | 4.2/6.7 |
| | 5 | 20.1/38.7 | 17.4/29.7 | 14.6/21.4 | 3.9/5.9 |
| Working condition 3 | 1 | 24.3/47.6 | 18.7/35.1 | 15.4/24.1 | 7.2/9.8 |
| | 2 | 22.1/43.1 | 15.4/21.4 | 13.7/25.6 | 6.9/8.7 |
| | 3 | 20.4/38.6 | 16.5/28.1 | 11.3/27.9 | 6.5/7.8 |
| | 4 | 21.6/35.8 | 17.8/29.7 | 13.2/28.4 | 6.2/6.7 |
| | 5 | 20.1/34.5 | 15.3/24.7 | 11.4/25.6 | 5.9/6.6 |

$$\mu_{ab}(x') = \exp\left(-\frac{(x' - c_{ab})^2}{2\sigma_{ab}^*}\right) \tag{9}$$

In Eq. 9, x' denotes the input value and $\mu_{ab}(x')$ denotes the degree of affiliation of x' belonging to the b th fuzzy set. c_{ab} and σ_{ab}^* denote the center and width of the a th input corresponding to the b th fuzzy set, respectively. The formula for the rule layer is shown in Eq. 10.

$$\begin{cases} Q_b = \prod_a \mu_{ab}(x'_a) \\ f_b(x') = p_b + \sum_a q_{ab} x'_a \end{cases} \tag{10}$$

In Eq. 10, both p_b and q_{ab} denote the rule parameters and Q_b denotes the activation of the b th rule. $f_b(x')$ denotes the output function of the b rule. Furthermore, the TSK fuzzy neural network has a fixed structure, therefore when dealing with a real-time changing motor SCS, the issue of uncertainty regarding the amount of neurons in the hidden layer leading to the RBF may still persist (Bensalem et al., 2022). Therefore, the study tries to self-learn the TSK network, and the self-learning process is shown in Figure 5.

In Figure 5, the initial data is first input to the front end of the TSK for fuzzification operation, while the center value calculation, width calculation and weight calculation of the first data are performed by the node parameter correction and approximation equations of the RBF neural network. At this point, these parameters are compared in the form of threshold judgment, if it is greater than the threshold then structure learning is performed, otherwise parameter learning is performed. After structure learning a new node is generated and the new node repeats the fuzzification operation and RBF parameter approximation calculation again. If the new parameters at this time are similar to the initial parameters, the new node is removed, unless the

parameters are significantly different, then it is chosen to be retained and parameter learning is performed along with the previous parameters. Finally, if these learned parameters are able to make the motor SCS stabilized then the parameters are output, otherwise the first step of the computation is repeated. The study proposes a novel parametric controller for sliding mode control of FPMSM speed control system, i.e., TSK-RBF-PID speed sliding mode controller. The control system is divided into three main parts, i.e., RBF parameter optimization module, TSK fuzzy neural network parameter tuning module, and PID speed controller. The flow of the model starts with five current signals output from the motor, which are first converted into digital signals by an analog-to-digital converter, i.e., ADC. The digital signal is processed by the Clark transform to obtain two orthogonal current components i_α and i_β for the α and β axes. These two components are subsequently further converted into d-axis and q-axis current components, i.e., i_d and i_q , by means of Pike transformations such as, i.e., Eq. 6. Two error controllers are added to this process to ensure that the current regulator accurately tracks and controls the target current in closed-loop control. In the control section, i_d and i_q are processed by two separate PI controllers to generate two control signals u_q and u_d , respectively. The reference voltages u_q and u_d are generated by the inverse Park transform to generate the voltage components in the α and β axes, which are then regulated by the current controller to finally generate i_q . The voltage components in the α and β axes are then regulated by the current controller. These control signals are then subjected to another Pike transformation and integrated into the final control signals u_α , u_β and T_k . These signals are further processed by the space vector pulse modulation technique and are used to control the speed and torque of the motor. In this case, the α -axis current component is converted to the α -axis current component i_α by Clarke transform, and then combined with the motor rotor angle θ

by Park transform, and finally converted to the d -axis current component i_d . e denotes the weights, e_ω denotes the corrected weights, and ω denotes the angular velocity at which the motor is running. When the value of the motor running angular velocity is input, the value output using the weights calculation is different from the desired value, and its error is utilized to make a reverse correction, thus reducing the error. The control quantity in this control process is the correction weights. At the same time, the angular velocity ω is used as the input data, and the correction weights e_ω are used as the control quantities, so that the proportional, differential, and integral values input into the PID controller can be calculated.

In addition, the model includes a feedback link where the difference between the actual speed of the motor and the set speed is calculated by the error detector and processed by the PID controller. Meanwhile, RBF parameter optimization and TSK fuzzy neural network are used to optimize the performance of the PID controller to ensure fast and accurate system response (Bensalem et al., 2021). The feedback control of the speed is done by a PID controller which optimizes the system response based on the speed error and its differentials. The RBF passes the optimized parameter information to the TSK fuzzy neural network for computation and finally feeds back to the PID controller for parameter updating and real-time control of FPMSM is implemented. Where the formula for the speed error is shown in Eq. 11.

$$e_{w'} = w'_{ref} - w'_{actual} \quad (11)$$

In Eq. 11, w'_{ref} denotes the desired speed of FPMSM and w'_{actual} denotes the actual speed of FPMSM. Eq. 12 displays the TSK fuzzy neural network's output at this stage.

$$\begin{cases} k_p(k) = k_p(k-1) + V k_p \\ k_i(k) = k_i(k-1) + V k_i \\ k_d(k) = k_d(k-1) + V k_d \end{cases} \quad (12)$$

The proportional gain, integral gain, and differential gain at the current time k are represented, respectively, by the letters $k_p(k)$, $k_i(k)$, and $k_d(k)$ in Eq. 12. The previous moment's proportional gain, integral gain, and differential gain are shown by the symbols $k_p(k-1)$, $k_i(k-1)$, and $k_d(k-1)$, respectively. The change amounts for proportional gain, integral gain, and differential gain are indicated by the letters $V k_p$, $V k_i$, and $V k_d$, respectively. The output of the PID controller at this time is shown in Eq. 13.

$$u(k) = u(k-1) + \sum_{m=p,i,d} k_m \hat{x}(m) \quad (13)$$

In Eq. 13, $u(k)$ denotes the output of the controller at moment k and k_m denotes the corresponding PID control gain at moment m . $\hat{x}(m)$ denotes the control error and related variables at the m moment. The PID controller can adapt dynamically to changes in the system thanks to this correction formula, preserving the system's performance and stability.

4 Experimental test

The experimental platforms for performance test and simulation test are built respectively, and firstly, the performance test is carried out for the software algorithm part in the TSK-RBF-PID Speed SMC

to compare with the same type of algorithmic model. Secondly, simulation tests are conducted on the TSK-RBF-PID controller to detect the parameter changes under different operating conditions.

4.1 TSK-RBF-PID speed sliding mode control performance test

The study starts with testing the TSK-RBF algorithm in TSK-RBF-PID Speed SMC. The operating system is set to Windows, the CPU is set to Intel Core i7, the GPU is NVIDIA RTX 1660s, and the memory is 16GB. The simulation modeling is implemented in MATLAB software, the momentum factor is set to 0.1, and the learning rate is 0.01. As the source of the test data, the PMSM dataset, a publicly available dataset used for motor troubleshooting, is selected. The public dataset contains the values of parameters such as rotational speed, torque, current, voltage, etc. Of the motor in normal state and fault state. It is divided into training and test sets according to the ratio of 8:2, while PT neural network algorithms that are more popular at this stage of FPMSM, such as Back Propagation (BP) neural network, RBF neural network, and Extreme Learning Machine (ELM), continue to be introduced. The algorithms are selected for their exemplary performance and adaptability in motor control. Among them, the BP network is well-suited for complex nonlinear mapping, the RBF network for rapid learning in real-time control, and the ELM is particularly suitable for rapid deployment. Additionally, the study optimizes the network parameters, such as the learning rate and the number of nodes, through cross-validation to ensure adaptation to the specific system dynamics, which yields the optimal performance of each algorithm. The parameter values of the PID speed controller are fixed, the target speed is set to 1,600 r/min, and 0–0.3 s is specified as the no-load start-up phase, and after 0.3 s as the stable output phase. Observe the change value of the motor speed curve under different algorithm models, and the specific test results are shown in Figure 6.

Figure 6A shows the variation curves of motor speed controlled by four different algorithms in the training set, and Figure 6B shows the variation curves of motor speed controlled by four different algorithms in the test set. From Figure 6, in the speed increase stage of the test set, the speed increase slope of TSK-RBF is the largest, and its fastest time to reach the target speed is 0.25 s. Although the slope of the training set is slightly lower than that of the separate RBF algorithm, the speed performance of TSK-RBF has been stable in the stabilized output stage, whereas the RBF leads to some fluctuations in the motor operation in the later stage due to the increase in the amount of overshooting. The rationale for this is that the TSK-RBF algorithm considers a greater number of system characteristics and dynamic changes during training, which enables more precise control of the motor speed and avoids unnecessary fluctuations during the testing phase. The study tested the expected parameter optimization with the better performing RBF and TSK-RBF, and the comparative results of the parameter optimization of the two algorithms are shown in Figure 7.

The expected and actual parameters of the RBF algorithm are compared in Figure 7A, and the outcomes of the TSK-RBF algorithm's comparison are compared in Figure 7B. In Figure 7, relatively speaking, among the 20 parameter optimization objective values, the RBF algorithm only exhibits a parameter optimization

rate of 50%, which is manifested by the low overlap between the expected and real parameters. On the contrary, the TSK-RBF algorithm proposed in the study has a parameter optimization rate of up to 90%. As the sample size increases, the degree of overlap between the expected and true parameters of the sample also increases significantly. This is due to the fact that the TSK-RBF technique is typically capable of modifying the TSK model's parameters and the RBF neural network's weights in real time, thereby improving the performance of adaptive speed regulation. In order to quantify the index performance effect under different algorithms, the study is conducted to compare the small and large inertia, i.e., the rotational inertia of the SCS is $2 \times 10^{-5} \text{kg}\cdot\text{m}^2$ and $5 \times 10^{-5} \text{kg}\cdot\text{m}^2$ as the established conditions, respectively, and the overshooting amount and the regulation time are taken as the indexes. To provide a comprehensive comparison, the most cutting-edge technology currently available in the field, namely, literature 18, is also included in the test. The results of this comparison are presented in Table 1.

As illustrated in Table 1, the Literature 18 proposed method exhibits superior performance in terms of both overshooting and adjustment time data when compared to BP and ELM. However, collectively, TSK-RBF demonstrates the most advantageous performance. Under small inertia conditions, the TSK-RBF controller overshoots by only 3% with a tuning time of 0.02 s, indicating that it provides the fastest system stability and the smallest overshoot under small inertia conditions. Under large inertia conditions, the TSK-RBF controller again performs best, with a significant drop in overshoot to 8%. The tuning time is 0.04 s. The rationale for this is that TSK-RBF enables the controller to predict and adjust to the optimal control parameters with greater precision. In this instance, the TSK model provides fine fuzzy logic control that automatically adjusts the control rules in accordance with the system dynamics. Furthermore, the RBF network optimizes the control parameters through its learning ability, particularly when the system load or dynamics change significantly, in order to facilitate rapid adaptation and the reduction of overshooting. The preceding data demonstrate that the TSK-RBF controller exhibits robust performance under diverse operational scenarios, particularly in the context of systems with substantial inertia. The lower overshoot means more precise control, and the shorter adjustment time indicates that the system is more responsive and can reach a steady state more quickly.

4.2 TSK-RBF-PID speed sliding mode control simulation test

The study used Matlab platform to build the controller of TSK-RBF-PID, in which the TSK fuzzy neural network is realized by sigmoid function. The network's learning rate is fixed at 0.05, its integral coefficient is 0.813, and its proportional coefficient in the PI coefficients is 2.615. The model of the motor used for the test is 6SZW40-90-15, the rated torque is 10T/(N·m), the rated rotational speed is set to 2700n/(r/min), the rotational moment of inertia is 0.0184J/(kg·m²), and the stator resistance is 2.15L/mH. Two different working conditions are set for the study, working condition 1 is set with a rated speed of 1,600 r/min and a load of 10N·m pair is applied abruptly at 0.5 s. Condition 2 sets the rated

speed to 1,600 r/min and changes the speed to 1,900 r/min at 0.5 s. Comparative tests of simple PID control, RBF neural network control, TSK-RBF fuzzy neural network control and TSK-RBF-PID control are carried out through the two conditions, and the results of the tests are shown in Figure 8.

The test results of the four control techniques in Condition 1 are displayed in Figure 8A, and the test results of the four control methods in Condition 2 are displayed in Figure 8B. The TSK-RBF-PID may initially and smoothly reach the normal goal speed in Figure 8A in 0.22 s. The next is the TSK-RBF control method with 0.23 s, and the slowest is the PID control method with 0.235 s. In addition, when the load is suddenly applied in the 0.5 s, the speed fluctuates the most for the PID control method with the speed decreasing by about 6%, and the recovery time is the longest at 0.08 s. Comparatively speaking, the TSK-RBF-PID control method has the smallest fluctuation, with a speed decrease of only 1% and the fastest recovery time of 0.02 s. The preceding results demonstrate that the combination of RBF and TSK optimizes the control strategy, enabling the controller to react promptly to sudden load or parameter changes and to rapidly restore the steady state. Furthermore, the study plots the current change curves of the four control techniques under the condition of working condition 1 to more graphically demonstrate the performance effect of various control methods, as illustrated in Figure 9.

Figures 9A, B, C, D depict the current variation curves under PID, RBF, TSK, and TSK-RBF control methods, respectively. They also depict the current variation curves under TSK-RBF-PID and TSK-RBF-RBF control methods. Where stage A is the motor start-up stage, stage B is the motor stable operation stage, and stage C is the recovery stage after impact. In Figure 9 in stage A, the TSK-RBF-PID control method shows a much smaller current variation, stabilized in the range of -10A – 10A , and its shortest time is 0.15 s. In stage B, from all four control methods show a more stable current. When the load is added at the beginning of 0.5 s, the current of the TSK-RBF-PID control method still fluctuates in the range of -10A – 10A , and its current state recovery time is the shortest of 0.2 s, which is nearly half of the data compared with the 0.4 s of the PID control method. The final study introduces hardware rolling bearings as test artifacts, employing control error and overshoot as reference indicators. Additionally, a new working condition environment is introduced to enhance the comprehensiveness of the test, designated as working Condition 3. The rated rotational speed is maintained at 1,600 r/min throughout the entirety of the process in working Condition 3. A total of five cycles of testing are conducted for each of the four control methods under the three working conditions, and the test results are presented in Table 2.

Table 2 illustrates that the TSK-RBF-PID control method exhibits the lowest control error among the four methods under working Condition 1, with a value of 3.7%. Additionally, its overshoot is the lowest among the methods, at 5.9%. This represents a notable decrease in overshoot compared to the other methods. In Condition 2, the TSK-RBF-PID control method also demonstrates superior performance, with the lowest control error of 3.9% and the lowest overshoot of 5.9%. In accordance with Condition 3, the TSK-RBF-PID control method continues to demonstrate optimal performance, with a control error of 5.9% and an overshoot of 6.6% representing the lowest values observed. In

conclusion, following numerous cycles of rolling bearing production tests, it has been demonstrated that the TSK-RBF-PID control method exhibits clear advantages in performance compared to other methods under these two operating conditions. Furthermore, it is more suitable for sliding mode control of FPMSM speed control systems at this stage.

5 Conclusion

SMC is frequently utilized in the study of SCSs for FPMSM in order to enhance the system's control performance. However, due to the nonlinearity and complexity of the SCS of FPMSM, the conventional SMC method may suffer from performance degradation in some cases. In light of the aforementioned considerations, the study employs Clark and Pike transformations to construct a mathematical model of FPMSM. Furthermore, the parameter parameterization of PID control is optimized through the integration of a RBF neural network and TSK fuzzy neural network. The experimental results demonstrated that the TSK-RBF control algorithm exhibits the greatest slope of motor speed increase and the fastest time to reach the target speed, with a rate of up to 90% for expected parameter optimization. Furthermore, the overshooting amount of the TSK-RBF controller in a small inertia working condition was only 3%, with a tuning time of 0.02 s. The TSK-RBF-PID control method exhibited minimal speed fluctuations in the presence of load torque, with a maximum speed drop of only 1% and the fastest recovery time of 0.02 s. Comparing with the same type of control methods, it was found that the TSK-RBF-PID controller had the lowest control error of 3.7%, the lowest overshooting amount of 5.9%. In conclusion, the TSK-RBF-PID control method not only enhances the adaptive capability of the control system, but also ensures high accuracy and fast response in a variable industrial environment. In addition, there are still some limitations in studying the proposed method, such as the effect of the added parameter tuning in the TSK fuzzy neural network on the real-time performance, which may affect the real-time performance of the controller. Future research could focus on optimizing the network structure and learning algorithm to

reduce the required parameter adjustments and improve the real-time performance and robustness of the control algorithm.

Data availability statement

The original contributions presented in the study are included in the article/Supplementary Material, further inquiries can be directed to the corresponding author.

Author contributions

JF: Conceptualization, Data curation, Formal Analysis, Investigation, Methodology, Project administration, Resources, Supervision, Validation, Writing—original draft, Writing—review and editing.

Funding

The author(s) declare that no financial support was received for the research, authorship, and/or publication of this article.

Conflict of interest

The author declares that the research was conducted in the absence of any commercial or financial relationships that could be construed as a potential conflict of interest.

Publisher's note

All claims expressed in this article are solely those of the authors and do not necessarily represent those of their affiliated organizations, or those of the publisher, the editors and the reviewers. Any product that may be evaluated in this article, or claim that may be made by its manufacturer, is not guaranteed or endorsed by the publisher.

References

- Abbassi, A., Ben Mehrez, R., Bensalem, Y., Abbassi, R., Kchaou, M., Jemli, M., et al. (2022). Improved arithmetic optimization algorithm for parameters extraction of photovoltaic solar cell single-diode model. *Arabian J. Sci. Eng.* 47 (8), 10435–10451. doi:10.1007/s13369-022-06605-y
- Abbassi, R., Saidi, S., Abbassi, A., Jerbi, H., Kchaou, M., and Alhasnawi, B. (2023). Accurate key parameters estimation of PEMFCs' models based on dandelion optimization algorithm. *Mathematics* 11 (6), 1298. doi:10.3390/math11061298
- Bensalem, Y., Abbassi, A., Abbassi, R., Jerbi, H., Alturki, M., Albaker, A., et al. (2022). Speed tracking control design of a five-phase PMSM-based electric vehicle: a backstepping active fault-tolerant approach. *Electr. Eng.* 104 (4), 2155–2171. doi:10.1007/s00202-021-01467-3
- Bensalem, Y., Kouzou, A., Abbassi, R., Jerbi, H., Kennel, R., and Abdelrahem, M. (2021). Sliding-mode-based current and speed sensors fault diagnosis for five-phase PMSM. *Energies* 15 (1), 71–72. doi:10.3390/en15010071
- Bi, G., Wang, Q., Ding, D., Li, B., and Zhang, G. (2022). Multi-optimization objective online tracking-based parameter self-tuning method for sensorless PMSM drives. *IEEE Trans. Transp. Electrification* 9 (1), 1390–1402. doi:10.1109/tte.2022.3200368
- Choudhuri, S., Adeniyi, S., and Sen, A. (2023). Distribution alignment using complement entropy objective and adaptive consensus-based label refinement for partial domain adaptation. *Artif. Intell. Appl.* 1 (1), 43–51. doi:10.47852/bonviewaia2202524
- He, H., Sun, F., Wang, Z., Lin, C., Zhang, C., Xiong, R., et al. (2022). China's battery electric vehicles lead the world: achievements in technology system architecture and technological breakthroughs. *Green Energy Intelligent Transp.* 1 (6), 100020. doi:10.1016/j.geits.2022.100020
- He, W., Wu, X., Chen, J., and Wang, Y. (2020). Comparative study of sensorless control of Permanent magnet synchronous motor realised by sliding-mode observer. *IET Power Electron.* 13 (6), 1191–1199. doi:10.1049/iet-pel.2019.1153
- Hou, Q., Ding, S., and Yu, X. (2020). Composite super-twisting sliding mode control design for PMSM speed regulation problem based on a novel disturbance observer. *IEEE Trans. Energy Convers.* 36 (4), 2591–2599. doi:10.1109/tec.2020.2985054
- Hussain, H. A. (2020). Tuning and performance evaluation of 2DOF PI current controllers for PMSM drives. *IEEE Trans. Transp. Electrification* 7 (3), 1401–1414. doi:10.1109/tte.2020.3043853

- Junejo, A. K., Xu, W., Mu, C., Ismail, M. M., and Liu, Y. (2020). Adaptive speed control of PMSM drive system based a new sliding-mode reaching law. *IEEE Trans. Power Electron.* 35 (11), 12110–12121. doi:10.1109/tpel.2020.2986893
- Li, J., Du, B., Zhao, T., Wu, S., and Cui, S. (2022). Current sensor fault-tolerant control for five-phase PMSM drives based on third-harmonic space. *IEEE Trans. Industrial Electron.* 69 (10), 9827–9837. doi:10.1109/tie.2022.3163541
- Li, X., Zhang, S., Cui, X., Wang, Y., Zhang, C., Li, Z., et al. (2021). Novel deadbeat predictive current control for PMSM with parameter updating scheme. *IEEE J. Emerg. Sel. Top. Power Electron.* 10 (2), 2065–2074. doi:10.1109/jestpe.2021.3133928
- Liu, Y. C., Laghrouche, S., Depernet, D., Djerdir, A., and Cirrincione, M. (2020). Disturbance-observer-based complementary sliding-mode speed control for PMSM drives: a super-twisting sliding-mode observer-based approach. *IEEE J. Emerg. Sel. Top. Power Electron.* 9 (5), 5416–5428. doi:10.1109/jestpe.2020.3032103
- Long, J., Yang, M., Chen, Y., Xu, D., and Blaabjerg, F. (2020). A novel voltage injection based offline parameters identification for current controller auto tuning in SPMSM drives. *Energies* 13 (11), 3010–3011. doi:10.3390/en13113010
- Mossa, M. A., Echeikh, H., and Ma'arif, A. (2022). Dynamic performance analysis of a five-phase PMSM drive using model reference adaptive system and enhanced sliding mode observer. *J. Robotics Control (JRC)* 3 (3), 289–308. doi:10.18196/jrc.v3i3.14632
- Sun, G., Yang, G., Su, J., and Lu, G. (2022). A flux-linkage torque ripple suppression method of dual-series fpmms decoupling control based on dual-frequency vector modulation. *Energies* 15 (13), 4700–4701. doi:10.3390/en15134700
- Xia, J., Li, Z., Yu, D., Guo, Y., and Zhang, X. (2020). Robust speed and current control with parametric adaptation for surface-mounted PMSM considering system perturbations. *IEEE J. Emerg. Sel. Top. Power Electron.* 9 (3), 2807–2817. doi:10.1109/jestpe.2020.3015288
- Xia, X., Zhang, B., and Li, X. (2020). High precision low-speed control for permanent magnet synchronous motor. *Sensors (Basel, Switz.)* 20 (5), 1526–1620. doi:10.3390/s20051526
- Xu, B., Zhang, L., and Ji, W. (2021). Improved non-singular fast terminal sliding mode control with disturbance observer for PMSM drives. *IEEE Trans. Transp. Electrification* 7 (4), 2753–2762. doi:10.1109/tte.2021.3083925
- Xu, W., Junejo, A. K., Liu, Y., Hussien, M. G., and Zhu, J. (2020). An efficient antidisturbance sliding-mode speed control method for PMSM drive systems. *IEEE Trans. Power Electron.* 36 (6), 6879–6891. doi:10.1109/tpel.2020.3039474
- Yang, C., Song, B., Xie, Y., and Tang, X. (2021). Online parallel estimation of mechanical parameters for PMSM drives via a network of interconnected extended sliding-mode observers. *IEEE Trans. Power Electron.* 36 (10), 11818–11834. doi:10.1109/tpel.2021.3067328
- Zhao, K., Leng, A., Zhou, R., Dai, W. K., Wu, S., and Li, T. (2021). Demagnetization fault reconstruction for six-phase permanent magnet synchronous motor by improved super-twisting algorithm-based sliding-mode observer. *Measurement* 172 (4), 108905–108906. doi:10.1016/j.measurement.2020.108905
- Zheng, S., Zhu, X., Xiang, Z., Xu, L., Zhang, L., and Lee, C. H. (2022). Technology trends, challenges, and opportunities of reduced-rare-earth PM motor for modern electric vehicles. *Green Energy Intelligent Transp.* 1 (1), 100012. doi:10.1016/j.geits.2022.100012